Stochastic Model-Based Left Ventricle Segmentation in 3D Echocardiography using Fractional Brownian Motion

Omar S. Al-Kadi[1,2], Allen Lu[3], Albert J. Sinusas[2], and James S. Duncan[2,3]

[1] King Abdullah II School for Information Technology, University of Jordan, Jordan
[2] Radiology and Biomedical Imaging, Yale University, New Haven, CT, USA
[3] Biomedical Engineering, Yale University, New Haven, CT, USA
omar.al-kadi@yale.edu

Abstract. A novel approach for fully-automated segmentation of the left ventricle (LV) endocardial and epicardial contours is presented. This is mainly based on the natural physical characteristics of the LV shape structure. Both sides of the LV boundaries exhibit natural elliptical curvatures by having details on various scales, i.e. exhibiting *fractal-like* characteristics. The fractional Brownian motion (fBm), which is a non-stationary stochastic process, integrates well with the stochastic nature of ultrasound echoes. It has the advantage of representing a wide range of non-stationary signals and can quantify statistical local self-similarity throughout the time-sequence ultrasound images. The locally characterized boundaries of the fBm segmented LV were further iteratively refined using global information by means of second-order moments. The method is benchmarked using synthetic 3D echocardiography time-sequence ultrasound images for normal and different ischemic cardiomyopathy, and results compared with state-of-the-art LV segmentation. Furthermore, preliminary results on real data from canine cases is presented.

1 Introduction

Accurate and reliable segmentation of the left ventricle (LV) is important for cardiac function analysis. In clinical practice, the segmentation task involves the delineation of LV endocardium and epicardium contours. This process, however, is tedious and time consuming. An automatic and robust approach for segmenting cardiac ultrasound time-sequences would highly facilitate the routine clinical work [1].

Several key challenges in the automated segmentation of the LV in cardiac ultrasound datasets exist. Namely, *speckle intensity heterogeneity*: as in LV blood pool due to blood flow or the dynamic motion of the heart; *obscureness*: close proximity of the papillary muscles tend to show speckle intensities similar to that of the myocardium; *spatial complexity of anatomy*: the separating border between right and left ventricle, and the low contrast between the myocardium and lung air may pose additional challenges for LV segmentation.

To address these challenges, it is advantageous to have an efficient segmentation algorithm that is objective and reproducible to accelerate and facilitate the process of diagnosis. Regarding ultrasound B-mode segmentation efforts, the endocardium and epicardium boundaries are delineated using a variety of strategies. In particular, statistical models which encode high-level knowledge, as the parametric or geometric deformable models, can handle topological changes robustly [2]. However, the model needs to be initialized sufficiently close to the object to converge and is sometimes prone to local minima. Taking advantage of unlabelled data for detecting data-driven features has drawn increased attention in prior probabilistic maps [3] and deep learning techniques [4]. However, limited training data is a common obstacle in the latter techniques, and regularization of the training data with a large amount of human-annotated data or anatomical models from large data sets is not always available. An intuitive approach would be to incorporate the spatiotemporal domain for improving structure and inter-dependencies of the output.

Dealing with the LV segmentation problem from a spatiotemporal perspective can give further information on the shape boundaries. Due to the nature of the speckle pattern, it is hard to draw conclusions about the boarder of the LV from still frames. Thus, cardiologist usually examine videos of the deformation of the LV wall during the echocardiographic examination. It is logical to assume the speckle pattern structure is better localized when the spatiotemporal coherence is considered. In this regard, Huang et al. exploits the spatiotemporal coherence of individual data for cardiac contour estimation [5]. Others embarked on introducing temporal consistency in the tracked speckle pattern using optical flow [7] or gradient vector flow approach [6]. Nevertheless, the spatiotemporal structures of the speckle patterns are usually stochastic in nature. Neglecting the inherent heterogeneity might not characterize the structure in space and time efficiently. The fractional Brownian motion (fBm), which is a non-stationary stochastic process, integrates well with the stochastic nature of ultrasound echoes [8]. It has the advantage of representing a wide range of non-stationary signals and can quantify statistical self-similarity in time-sequence ultrasound images.

To address the aforementioned challenges, we present a novel physically motivated stochastic model for improved epicardium and endocardium boundary segmentation. Motion roughness, reflected in the speckle pattern, is characterized by fBm for local boundary delineation – which is theoretically invariant to intensity transformations [9]. Using second-order moments for LV shape global information complements the local characterization of the fBm process.

2 Methods

2.1 Fractional Brownian motion

Brownian motion $B(t)$ is a *Markovian* process, whose conditional transition density function is time-homogeneous. Based on the Lagrangian representation, the generalization of a standard $B(t)$ is a Fractional Brownian motion $B_H(t)$, which

is a continuous Gaussian self-similar process in $\mathbb{R}$ with stationary increments [10]. $B_H(t)$ can be modeled via stochastic integral equation, given by

$$B_H(t) - B_H(0) = \frac{1}{\Gamma(H+\frac{1}{2})}\Big\{ \int_{-\infty}^{0} (t-s)^{H-1/2} - (-s)^{H-1/2} dB(s) + \int_{0}^{t} (t-s)^{H-1/2} dB(s)\Big\}, \quad (1)$$

where $\Gamma(x)$ and $B(t)$ are the gamma function and standard Brownian motion, respectively, and $H \in (0,1)$ is called the Hurst index which describes the scaling behaviour of the process and the roughness of the resultant motion or trajectory [11]. For our case, H characterizes the deformation of the left ventricle wall motion, with lower values leading to a heterogeneous motion and vice versa. From (1), the standard $B(t)$ is recovered when $H = \frac{1}{2}$. But in contrast, fBm has dependent increments when $H \neq \frac{1}{2}$. By allowing H to differ from $\frac{1}{2}$, a fBm process is achieved, where for $H > \frac{1}{2}$ increments are positive correlated, and for $H < \frac{1}{2}$ increments are negatively correlated.

A normalized fractional Brownian motion $\{B_H(t), t \in \mathbb{R}^N\}$ with $0 < H < 1$ is uniquely characterized by the following properties: (a) $B_H(t)$ has stationary increments; (b) $B_H(0) = 0$, and $\mathbb{E}[B_H(t)] = 0$ for $t \geq 0$; and (c) $\mathbb{E}[B_H^2(t)] = t^{2H}$ for $t \geq 0$; then it follows that the covariance function is given by

$$\rho(s,t) = \mathbb{E}(B_H(s)B_H(t)) = \frac{1}{2}\big[|t|^{2H} + |s|^{2H} - |t-s|^{2H}\big], \quad \forall\ s,t \in \mathbb{R}^N, \quad (2)$$

for $0 < s \leq t$, where $\mathbb{E}$ denotes the expectation operator with respect to probability space, and $|t|$ is the Euclidean norm of $t \in \mathbb{R}^N$.

2.2 Fractal Dimension Estimation

There are several ways to estimate the fractal dimension (FD) of a stochastic process modeled by a fBm [9]. All of them are based on the formula

$$\mathbb{E}\Big[(\tilde{B}_H(n+t) - \tilde{B}_H(n))^2\Big] = \sigma^2(t)^{2H}, \quad (3)$$

for the variogram of fBm, which follows from (2), and σ^2 represents the variance of the increments. The fBm and power-law variogram fits were used to estimate H as a measure of self-similarity. Then the discrete-time fBm process $\tilde{B}_H(n)$ after taking the logarithm of (3) yields the linear equation

$$\log \mathbb{E}\Big[(\tilde{B}_H(n+s) - \tilde{B}_H(n))^2\Big] = H \log|s| + \log c. \quad (4)$$

where c is proportional to the standard deviation σ.

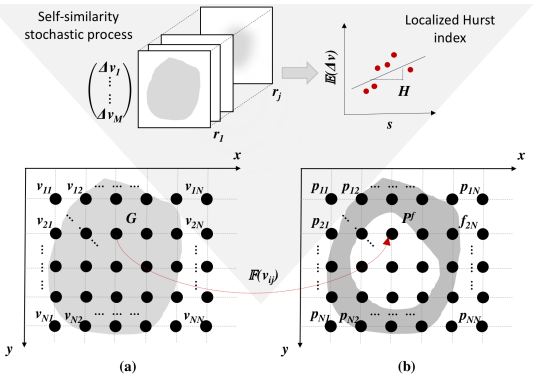

Fig. 1: Multiscale parametric mapping based on fractional Brownian motion (B_H) for voxel-based segmentation. (a) Object G having a spatial support $v_{1,1} \times v_{N,N}$ in source image $f_{x,y}$, and (b) constructed fractal parametric map $\mathcal{F}$ at different scales (r) representing localized Hurst indices (H).

The linearly-related H can be calculated from the slope of the average absolute difference plotted as a function of the increments n with step-size k on a log-log plot. The FD of an m-dimensional fBm is related to the Hurst index by $\mathrm{FD} = m - H$, where m is the Euclidean dimension, or the number of independent variables, and H quantifies the self-affinity of the process. Thereby, closer H is to one, the lower the the FD, and the smoother the process becomes and vice versa. Finally the parametric fractal dimension volume ($\mathcal{F}$) is generated voxel-by-voxel, represented as:

$$\mathcal{F}^{(i,r)} = \begin{pmatrix} m_1 \\ m_2 \\ \vdots \\ \vdots \\ m_M \end{pmatrix} - \begin{pmatrix} h^i_{11L} & h^i_{12L} & \cdots & \cdots & h^i_{1NL} \\ h^i_{21L} & h^i_{22L} & \cdots & \cdots & h^i_{2NL} \\ \vdots & \vdots & \ddots & & \vdots \\ \vdots & \vdots & & \ddots & \vdots \\ h^i_{M1L} & h^i_{M2L} & \cdots & \cdots & h^i_{MNL} \end{pmatrix} \tag{5}$$

where M, N and L are the volume elements defined in 3D space for each ultrasound time-sequence i, and $r = 1, \ldots, j$ is the resolution limits of $\mathcal{F}^{(i,r)}$ which represents the mean absolute intensity difference to center voxels defined as local range dependence (i.e. how far the resolution of r can be deeply probed). Fig. 1 illustrates the fractional Brownian motion (fBm) segmentation process.

Classification: Patches of 6.3×8.1 mm^2 – representing myocardium vs blood pool – were selected randomly from a single ultrasound volume transformed to $\mathcal{F}$, and used for training data. Such that, the training set, S_T, is composed of a set of N patches for which the feature vector [V–(5)], and the classification result (C_1 or C_2: myocardium or blood pool) are known $S_T = \{(V^{(n)}, C_k^{(n)} | n =$

$1, \ldots, N; k \in \{1, 2\}\}$. The Hurst index is a useful statistical method for inferring the properties of a time series without making assumptions about stationarity. It is most useful when used in conjunction with other techniques. Thus, features representing the mean FD, lacunarity – which defines the sparsity of the fractal pattern – and first and higher order statistics (skewness, kurtosis and variance) were derived from $\mathcal{F}$ to form a vector in a 5-D feature space $V = (v_1, v_2, \ldots, v_5)$. Then in the classification procedure, one of the classes C_1 (myocardium) or C_2 (blood pool) would be assigned to each candidate voxel when its representation is known. A Bayesian classifier was used for classification, although SVM or random forests would have also served the purpose.

2.3 Contour structuring moments

Image moments are defined as weighted averages of voxel intensities. For the time-sequence 3D ultrasound images, at time t and depth z, the raw (p, q)-moment $m_{p,q}$ for an fBm segmented object G (LV for our case) is given by:

$$m_{pq} = \sum_{x=1}^{N} \sum_{y=1}^{N} x^p y^q f(x, y), \tag{6}$$

where N is the size of G and $f(x, y)$ are the gray levels of individual voxels.

The first-order moments $m_{1,0}$ and $m_{0,1}$, when normalized by $m_{0,0}$ give the coordinates of the binary object – x_c and y_c of the endocardium or epicardium. Accordingly, second-order moments describe the "distribution of mass" with respect to the coordinate axes and define the orientation θ of G. In order to extracting the parameters of the equivalent ellipse from the second-order moments $m_{2,0}$, $m_{1,1}$, and $m_{0,2}$, the central moments can be defined as

$$\mu_{pq} = \sum_{p,q \in G}^{N} (x - x_c)^p (y - y_c)^q, \tag{7}$$

such that

$$\mu_{2,0} = \frac{m_{2,0}}{m_{0,0}} - x_c^2, \quad \mu_{1,1} = 2(\frac{m_{1,1}}{m_{0,0}} - x_c y_c), \quad \mu_{0,2} = \frac{m_{0,2}}{m_{0,0}} - y_c^2, \tag{8}$$

where x_c and y_c are the coordinates of the centroid c of G. These moments are invariants to translation. Then the eigen vectors of the covariance matrix of G correspond to the major l and minor w axes lengths with a certain angle θ for the equivalent ellipse. In this work, c was first identified on the fBm segmented LV base image, and used afterwards for alignment – through the rest of image sequence – towards the apex.

3 Experimental Results

Synthetic and Animal Data Validation was done on 5 different 3D ultrasound time-sequences from the KU Leuven synthetic data set [12], representing 1 normal and 4 ischemic. Each image had $224 \times 176 \times 208$ voxels of size $0.7 \times 0.9 \times 0.6$

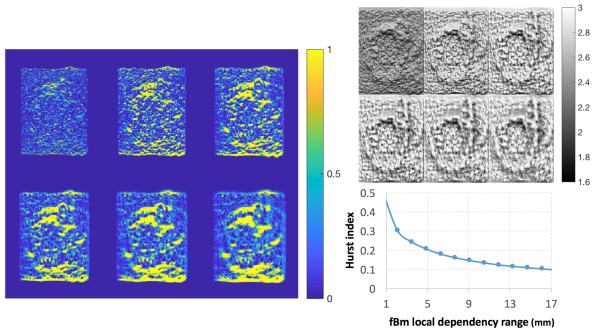

Fig. 2: fBm parameter estimation discrepancy by [left] residual sum of squares (RSS) for [right-top] corresponding fractal dimension parametric images; [right-bottom] change of RSS error for different fBm range dependence.

mm^3. For each sequence, ground truth motion trajectories were provided at 2250 mesh points. The endocardium and epicardium meshes were then converted into segmentation masks and used for benchmarking. Also, 3D ultrasound sequence images were acquired from 2 acute canine studies (open chested) following a severe occlusion of the left anterior descending coronary artery. A Philips iE33 ultrasound system with an X7-2 probe was used for image acquisition. Images typically had $400 \times 140 \times 120$ voxels of $0.25 \times 0.85 \times 0.85$ mm^3 with an average of 23 temporal frames. All experiments were conducted in compliance with the Institutional Animal Care and Use Committee policies.

Evaluating Model Goodness-of-Fit: The residual sum of squares (RSS) was used to measure the discrepancy in the estimated H indices of the parametric volume maps ($\mathcal{F}$). A smaller value indicates the model has a smaller random error component. Fig. 2 shows where errors most likely occur when locally computing H, and hence the estimation of $\mathcal{F}$. The size of the fBm localized range dependence in (5) was adjusted in the range between 0.7×0.9 and 9.1×11.7 mm^2. Higher RSS was encountered in longer range dependence as the introduced error may get accumulated due to echo artifacts. Also, Fig.2 shows how H values vary at different fBm local dependence ranges. Selecting the best fBm dependence range can avoid unnecessary computational time and give better accuracy.

Quantitative Evaluation: The proposed fBm segmentation method was benchmarked using Huang et al.'s method [5], which is based on employing spatiotemporal coherence under a dynamic appearance model (C-DAM). The evaluation of the segmentation quality was performed using Dice coefficient, and computed for both end-diastolic and -systolic and averaged over all cases, see Table 1.

One of the key properties of fBm is that it can exhibit persistence ($H > \frac{1}{2}$) or anti-persistence ($H < \frac{1}{2}$). Persistence is the property that the LV wall motion

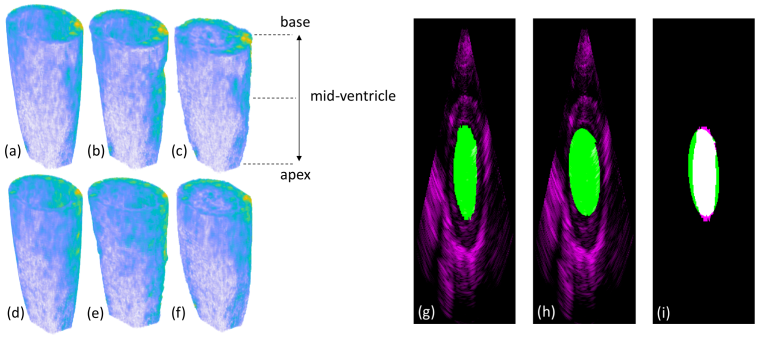

Fig. 3: [Left] 3D segmentation of left ventricle for time-sequence ultrasound images illustrating (a)-(c) ground truth, fBm, C-DAM for normal condition, and (d)-(f) ground truth, fBm, C-DAM for ischemic-Ladprox; [Right] canine endocardium segmentation of LV mid-slice for (g)-(i) manual, fBm-based, and comparing segmentation accuracy, respectively.

Table 1: Endocardium (E_n) and Epicardium (E_p) segmentation quality using Dice Coefficient for normal and ischemic cardiomyopathy

	Left Ventricle Condition				
Method	Normal	LADprox	LADdist	LCX	RCA
Our fBm (E_n)	0.87 ± 0.02	0.85 ± 0.02	0.84 ± 0.04	0.87 ± 0.02	0.88 ± 0.02
C-DAM (E_n)	0.84 ± 0.07	0.86 ± 0.03	0.84 ± 0.05	0.82 ± 0.04	0.85 ± 0.05
Our fBm (E_p)	0.92 ± 0.02	0.90 ± 0.02	0.88 ± 0.04	0.92 ± 0.02	0.93 ± 0.02
C-DAM (E_p)	0.91 ± 0.03	0.88 ± 0.02	0.93 ± 0.02	0.89 ± 0.04	0.88 ± 0.02

tends to be smooth, e.g. near to normal. Anti-persistence is the property that the relative stochastic process is very noisy, and hence LV wall motion trajectories tend to be heterogeneous. The latter case is an example of cardiac ischemia, such that displacements over one temporal or spatial interval are cancelled out by displacements over another time interval. From Table 1, the fBm segmentation method showed improved performance for 4 out 5 of both tested LV endo- and epicardium deformation conditions. Moreover, to visually demonstrate practical relevance, Fig. 3 shows the 3D segmentation of the LV and the mid-slice for the synthetic and canine data, respectively. Improved delineation of the epi- and endocardium boundaries can be seen, especially for the LV base slice.

4 Conclusion

This work presents a novel method for improving LV segmentation by addressing the problem of speckle pattern heterogeneity, where a) the fBm classification-

based segmentation method relies naturally on the spatiotemporal dependencies of the local features; b) the 3D sequence of Hurst indices, which was used to derive fractal dimension volume maps, are invariant to intensity transformations; c) global information about the LV shape using second-order moments complements the local characterization of the fBm process. Both local and global boundary information about the LV shape boundaries was captured with improved precision. Finally, we believe the relative complexity encountered in the animal study can be better dealt with if the segmentations were based on the radio-frequency envelope detected echos, which may better reflect the intrinsic properties of the myocardium tissue.

References

1. Frangi, A., Niessen, W., Viergever, M.: Three-dimensional modeling for functional analysis of cardiac images: A review. IEEE T Med. Imag. **20** (1), 2–25 (2001)
2. Carneiro, G., Nascimento, J. C.: Combining multiple dynamic models and deep learning architectures for tracking the left ventricle endocardium in ultrasound data. IEEE T Pattern Anal. Mach. Intell. **35**(11), 2592–2607 (2013)
3. Hansson, M. et al.: Segmentation of B-mode cardiac ultrasound data by Bayesian Probability Maps. Med. Imag. Anal, **18**(7), 1184–1199 (2014)
4. Carneiro, G., Nascimento, J. C., Freitas, A.: The segmentation of the left ventricle of the heart from ultrasound data using deep learning architectures and derivative-based search methods. IEEE T. Imag. Proc. **21**(3), 968–982 (2012)
5. Huang, X. J., et al.: Contour tracking in echocardiographic sequences via sparse representation and dictionary learning. Med. Imag. Anal. **18**(2), 253–271 (2014)
6. Zagrodsky, V., Walimbe, V., et al.: Registration-assisted segmentation of real-time 3-D echocardiographic data using deformable models. IEEE T. Med. Imag. **24**(9), 1089–1099 (2005)
7. Barbosa, D., Friboulet, D., D'hooge, J., Bernard, O.: Fast tracking of the left ventricle using global anatomical affine optical flow and local recursive block matching. In: Proc. MICCAI CETUS Challenge (2014)
8. Al-Kadi,O. S., Chung, D. Y.F., et al.: Quantification of ultrasonic texture intra-heterogeneity via volumetric stochastic modeling for tissue characterization. Med. Imag. Anal. **21**(1), 59–71 (2015)
9. Al-Kadi,O. S.: Fractals for biomedical texture analysis. In: Biomedical Texture Analysis: Fundamentals, Tools and Challenges. Academic Press. London. 131–161 (2017)
10. Mandelbrot, B.: Fractals and Chaos: The Mandelbrot Set and Beyond. Springer-Verlag. New York (2004)
11. O'Malley, D., Cushman, J.: Two-scale renormalization-group classification of diffusive processes. Phys. Rev. E. **86**(1), 011126–7 (2012)
12. Alessandrini, M., Heyde, B., et al.: Detailed evaluation of five 3D speckle tracking tlgorithms using synthetic echocardiographic recordings. IEEE T Med. Imag. **35**(8), 1915–1926 (2016)